Int. J. Environ. Sci. Technol. (2015) 12:1613–1624
DOI 10.1007/s13762-014-0730-9

ORIGINAL PAPER

Tin(IV) oxide nanoparticles grafted with *N*,*N*-dimethylacrylamide–allyl butyl ether for xylene adsorption

A. Beheshti Ardakani · H. A. Panahi · A. H. Hasani · A. H. Javid · E. Moniri

Received: 21 May 2014 / Revised: 6 October 2014 / Accepted: 6 December 2014 / Published online: 20 January 2015

Abstract This study presents a two-stage method for modification of tin(IV) oxide using (3-mercaptopropyl) trimethoxysilane and grafting of *N*,*N*-dimethylacrylamide-allyl butyl ether copolymer. The resulting sorbent was characterized by Fourier transform infrared spectroscopy, elemental analysis, thermogravimetric analysis, transmission electron microscopy, scanning electron microscopy, and the Brunauer–Emmett–Teller method and evaluated for xylene adsorption from environmental water samples. Batch experiments were conducted to evaluate the effect of the analytical parameters of pH, contact time, initial concentration and temperature. The optimum pH was 5, contact time was 5 min, and temperature for sorption of xylene was 30 °C. The capacity of the sorbent was 8.56 mg g^{-1}. Results showed good accessibility of the active sites. The equilibrium adsorption data of xylene sorption onto grafted nano-tin(IV) oxide were analyzed using the Langmuir, Freundlich, Temkin, and Redlich–Peterson isotherm models. The adsorption data were modeled as pseudo-first-order, pseudo-second-order, and intra-particle diffusion kinetic equations. The results show that adsorption followed by the Langmuir isotherm and the pseudo-second-order model and intra-particle diffusion model showed more than one process is controlling the adsorption process. The sorbent removed more than 90 % of the xylene from the water solution samples.

Keywords Xylene · Adsorption · Nanoparticles · Tin(IV) oxide · Modification · Grafting

A. Beheshti Ardakani · A. H. Hasani (✉)
Department of Environment and Energy, Science and Research Branch, Islamic Azad University, Tehran, Iran
e-mail: Hasani.amirhesam@yahoo.com

H. A. Panahi
Department of Chemistry, Central Tehran Branch, Islamic Azad University, Tehran, Iran

A. H. Javid
Department of Marine Science and Technology, Science and Research Branch, Islamic Azad University, Tehran, Iran

E. Moniri
Department of Chemistry, Varamin (Pishva) Branch, Islamic Azad University, Varamin, Iran

Introduction

Benzene, toluene, ethylbenzene, and xylene (BTEX) are petroleum volatile monoaromatic hydrocarbon compounds found in petroleum, gasoline, and industrial solvents that are environmental pollutants (Aivalioti et al. 2010). One of BTEX aromatic compounds classified as a priority toxic compound by the WHO is xylene (World health organization 2004). Xylene is discharged into the aqueous environment and makes water and wastewater resources inappropriate for use and human consumption (Aivalioti et al. 2010; Su et al. 2010). Chemical oxidation, air stripping, biological treatment, adsorption (Aivalioti et al. 2012a), and bioremediation (Kee et al. 2014; Silva-Castro et al. 2012) have all been used to remove xylene from water and wastewater. Of these, adsorption is most frequently employed.

Many absorbents can be used for adsorption of xylene from aqueous solutions, including carbon nanotubes, organoclay, activated carbon, diatomites, and nano-sorbents (Aivalioti et al. 2012b; Lin and Huang 1999; Nourmoradi 2012). Nano-materials have interesting properties that differ from those of their corresponding bulk states which make them promising sorbents in aqueous solutions

(Paraguay-Delgado et al. 2005; cheng et al. 2004). Recently, a great deal of attention has been focused on the synthesis and application of nanostructure materials as adsorbents to remove pollutants from water (Shahriari et al. 2014). Surface modification of nano-materials by grafting of polymer chains enhances their structural properties and sorption capacity (Ahmad Panahi et al. 2013).

The present study focuses on removing xylene from aqueous solutions by synthesizing an efficient nano-sorbent. Tin(IV) oxide (SnO_2) nanoparticles were synthesized using the co-precipitation method; after modification by 3-mercaptopropyl trimethoxysilane, they were grafted with *N*,*N*-dimethylacrylamide and allyl butyl ether. The performance of this grafted synthesized nano-sorbent was then investigated for use in xylene adsorption from water. The optimal conditions, three isotherm and three kinetic models, and the adsorption mechanism were evaluated. This research and all testing were carried out at the Tehran Science and Research branch of Islamic Azad University in 2014.

Materials and methods

Instruments

The pH measurements were done using a bench-top electrochemistry meter (Meridian series, Denver Instruments, Colorado, USA). The UV spectra of the samples were recorded at $\lambda = 264$ nm with a UV/Vis spectrophotometer (Jasco, V-630, Maryland, USA). Fourier transform infrared (FTIR) spectroscopy was carried out using a spectroscope (Jasco, model 410, Maryland, USA). Thermogravimetric analysis (TGA) measurements were recorded on a TGA-50H (Shimadzu, Kyoto, Japan). Transmission electron microscopy (TEM) images were recorded using a CM-200 transmission electron microscope, and scanning electron microscopy (SEM) was obtained on a XL30 microscope (Philips, Amsterdam). Elemental analysis was carried out on a thermo-elemental analyzer (model Flash EA, Finnigan, Milan, Italy). Nitrogen (N_2) adsorption–desorption was carried out at 195 °C (77 K) to determine the surface area, volume, and width of the AD-GNS micropores from Brunauer–Emmet–Teller (BET) adsorption using an automated gas sorption system (Micromeritics, Model ASAP 2020, USA).

Reagents and solutions

$SnCl_2.2H_2O$ and NH_3 applied for nano-SnO_2 synthesis were obtained from Merck (Darmstadt, Germany). For modification and grafting, 3-mercaptopropyl trimethoxysilane, allyl butyl ether (ABE), 2,2′-azobis (2-methylpropionittrile), and *N*,*N*-dimethylacrylamide (DMAA) were purchased from Sigma-Aldrich. Xylene (99 % pure), $C_4H_8O_2$, C_2H_5OH, HCl, NaH_2PO_4, Na_2HPO_4, CH_3COOH, CH_3COONa, NaOH, H_2SO_4, and HNO_3 were purchased from Merck (Darmstadt, Germany).

All reagents were in analytical grade and used without further purification. To adjust solution pH, 0.1 M acetate and phosphate buffer were used. A stoke solution (1,000 mg l^{-1}) of xylene was prepared by dissolving an appropriate amount of xylene in deionized water.

Synthesis of SnO_2 nanoparticles grafted with hydrophobic groups

Synthesis of nano-SnO_2

Methods for synthesis of nano-SnO_2 include the sol–gel method, spray pyrolysis, solvothermal routes, and co-precipitation (El-Etre and Reda 2010). In the present study, high volumes of SnO_2 nanoparticles were synthesized using the low-cost chemical co-precipitation method. The challenge for this method is that when the product is calcined at high temperatures the crystallite size increases and the surface area decreases in response to particle growth (Fujihara et al. 2004; Liang et al. 2007). The size of the SnO_2 nanoparticles was concernedly controlled by varying the reaction temperature and through the surface modifications (Ying et al. 2004).

Temperature and pH are the main factors that influence synthesis of smaller and more dispersed SnO_2 nanoparticles by chemical precipitation (Gaber et al. 2013). The size of the nano-SnO_2 particles increased slightly in response to surface modification. First, $SnCl_2.2H_2O$ (116.3 g) was dissolved in 250 ml distilled water to prepare 2 M $SnCl_2.2H_2O$ solution. Next, 2 M NH3 solution was added gradually to the $SnCl_2$ solution while stirring at room temperature (25 °C) to reach pH 7. The slurry was stirred for 2 h and then filtered. The precipitation was dried for 15 h at 100 °C. The size of the nanoparticles was successfully confined to 30–50 nm, which was suitable for the next stage. The resulting nano-SnO_2 was characterized by FTIR, elemental analysis, SEM, and TGA.

Polymer grafting

Free radical polymerization and anionically initiated polymerization are the two most common methods for graft polymerization onto inorganic oxide supports (Ahmad Panahi et al. 2010; Panahi et al. 2013). Radical polymerization has significant advantages over ionic and coordination polymerization. The reaction conditions are usually less demanding and exhibit tolerance of trace impurities,

and it is possible to polymerize a variety of monomers (Chiefari et al. 2003).

In free radical grafting onto inorganic compound like SnO_2, modification of the surface is required by bonding reactive sites with either initiator or reactive functional groups (Chaimberg and Cohen 1990). Synthesizing a sorbent with controlled surface properties using selected functional groups is the most important aspect of grafting. A two-stage method was utilized (Ahmad Panahi et al. 2013) for this step. The first stage was modification of SnO_2 with 3-mercaptopropyl trimethoxysilane, and second stage was grafting the DMAA-ABE copolymer onto the modified SnO_2.

Modification of SnO_2 nanoparticles with 3-mercaptopropyl trimethoxysilane

SnO_2 nanoparticles were silylated using an anhydrous solution of 5 % 3-mercaptopropyl trimethoxysilane in 1,4-dioxane. A mixture of SnO_2 nanoparticles (3 g), 1,4-dioxane (2.5 ml), and 3-mercaptopropyl trimethoxysilane (47.5 ml) was refluxed for 24 h at 100 °C. The solid precipitate was filtered and washed several times with 30 ml of 1,4-dioxane and dried under vacuum in a desiccator over dry calcium chloride.

Graft polymerization

Free radical graft polymerization of ABE and DMAA onto modified SnO_2 nanoparticles was done in a temperature-controlled reactor under stirring in a nitrogen atmosphere. Nitrogen helps to exclude oxygen, which causes the formation of acetaldehyde, a well-known chain transfer agent (Chaimberg and Cohen 1990). In this stage, a mixture of modified SnO_2 nanoparticles (3 g), ethanol (30 ml), ABE (4 ml), DMAA (1 ml), and 2,2′-azobis (2-methylpropionittrile) (0.1 g) was prepared, and the mixture was refluxed in a nitrogen atmosphere for 8 h at 65 °C. The grafted SnO_2 nanoparticles were filtered and washed with ethanol and water several times to remove any homopolymer that may have been absorbed and then dried under vacuum in a desiccator over dry calcium chloride. The methodology of the poly-grafted (ABE-co-DMAA) nano-SnO_2 (AD-GNS) is shown in Fig. 1. The AD-GNS was characterized by FTIR, elemental analysis, TGA, TEM, and SEM.

pH of point of zero charge (pH_{ZPC})

The point of zero charge (PZC) of AD-GNS was determined by the solid addition method as described by Vieira et al. (2009). Eight vials containing solutions with pH values of 3–9 (pH_0) and 0.10 g of AD-GNS were shaken for 24 h at room temperature, and the final pH was determined. The difference between the initial and final pH (ΔpH) was plotted against pH_0 and the point at which $\Delta pH = 0$ was recorded as pH_{zpc}.

Batch method of xylene adsorption

A set of solutions (each 25 ml) containing 0.145 ml xylene was prepared and their pH values adjusted to the optimum value of 5. Then, 0.02 g of grafted nano-SnO_2 was added to each solution, and the solution was shaken for the optimum time of 5 min. The sorbent was filtered, the suspensions were centrifuged at 6,000 rpm for 15 min, and the clear supernatant was analyzed using a UV/Vis spectrophotometer.

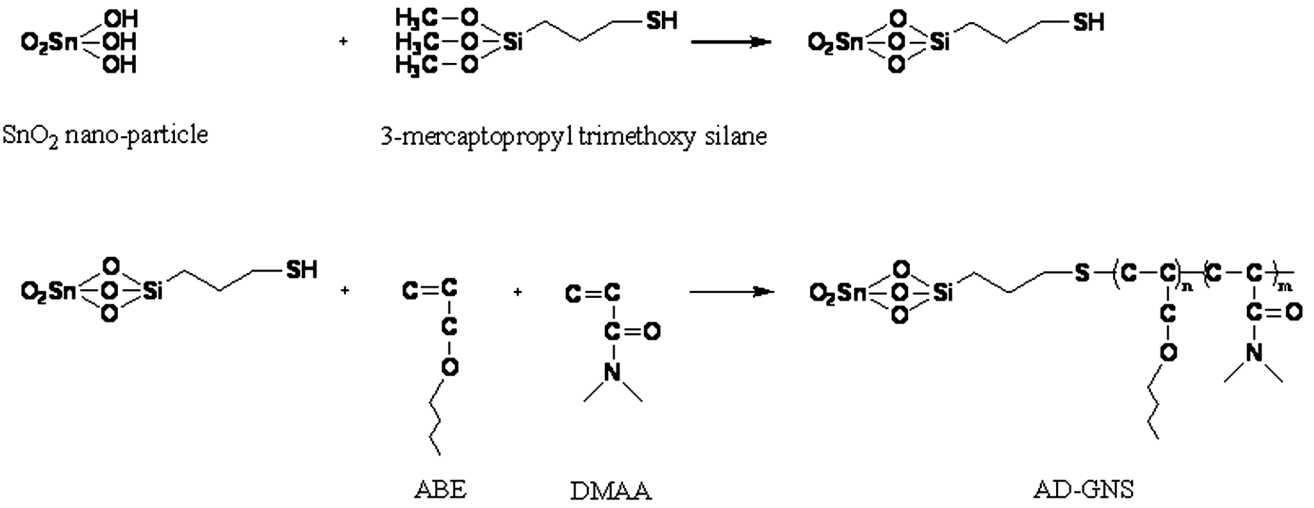

Fig. 1 Schematic presentation of synthesis and grafting process of AD-GNS

Isotherm studies

Isotherm studies were carried out by adding 0.01–0.07 g grafted nano-sorbent to the samples (each 25 ml containing 0.145 ml xylene-5 μg l^{-1} solution). The samples were then sealed and placed in a vortex for 2 h at pH 5 at 25 °C. The samples were centrifuged, and the final concentration of xylene in the supernatant was measured using a UV/Vis spectrophotometer. The amount of xylene at equilibrium q_e (mg/g) on the grafted nano-SnO_2 was calculated as:

$$q_e = (c_0 - c_e)V/W \quad (1)$$

where C_0 and C_e(mg g^{-1}) are the initial and equilibrium concentrations of xylene, V(L) is the volume of the solution, and $W(g)$ is the mass of the AD-GNS.

Results and discussion

Characterization of AD-GNS

The AD-GNS was characterized by FTIR, elemental analysis, TGA, TEM, and SEM. FTIR of the SnO_2 nanoparticles confirmed the presence of Sn–O–Sn at about 617 cm^{-1} and O–H at 3,421 cm^{-1}. Modification with 3-mercaptopropyl trimethoxysilane was confirmed by a peak at 1,091 cm^{-1} caused by the Si–O band in the FTIR of the modified SnO_2 nanoparticles. The presence of CH_2, CH, and OH is indicated at 1,430, 2,937, and 3,436 cm^{-1}, respectively. The IR spectrum of the AD-GNS was compared with that of the modified SnO_2 nanoparticles. Two additional bands appear at about 1,103 and 1,641 cm^{-1} that correspond to C–O and C=O, respectively.

The TGA of the nano-SnO_2 shows weight loss up to 600 °C caused mainly by desorption of water molecules from the surface. AD-GNS shows two phases of weight loss, one up to 200 °C and one at 200–600 °C caused by water molecule desorption and polymeric matrix decomposition, respectively. This confirms the grafting of the copolymers onto the nanoparticles.

The elemental analysis of AD-GNS showed 55.27 % C, 5.72 % H, and 3.13 % N, which confirms the polymeric construction of the synthesized sorbent. The presence of N proves that DMAA molecules were in the repeating unit of the polymer. TEM shows spherical agglomerated microparticles with diameters of less than 100 nm. The polymer morphology was surveyed using SEM before and after graft polymerization. Figure 2a shows the smooth and homogenous appearance of the SnO_2 nanoparticle surface and the absence of heterogeneity or cracking. As shown in

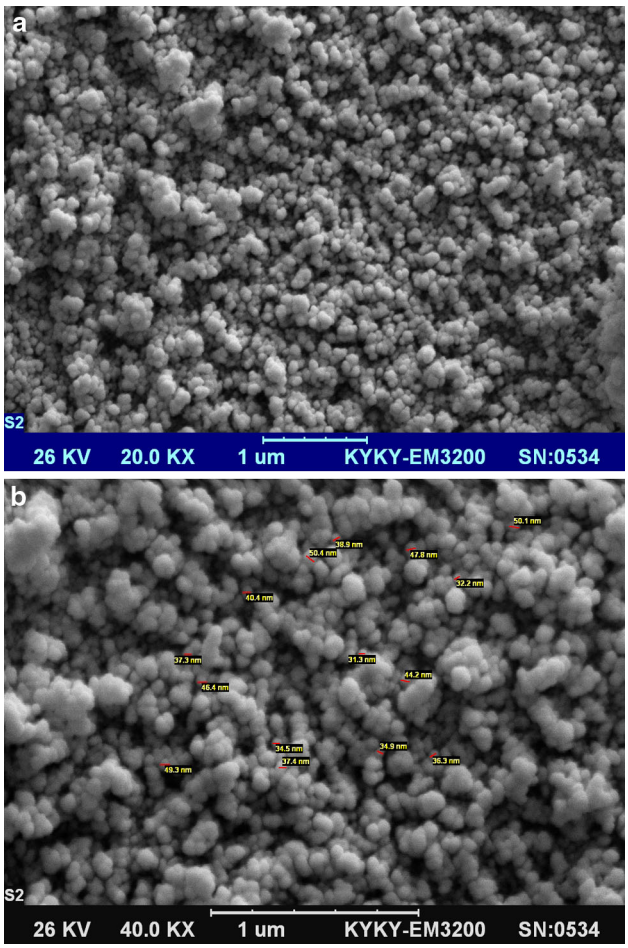

Fig. 2 SEM images of: **a** SnO_2 nanoparticles; **b** AD-GNS

Fig. 2a, b, when SnO_2 nanoparticles were grafted with polymer chains containing ABE and DMAA, the surface became slightly coarser, but remained homogenous. SEM shows that particle size for AD-GNS was ranged from 30 to 50 nm.

Sites available for adsorption can be identified by modeling the adsorption of gases by a porous sorbent and measuring surface area, pore volume, and width (Gusmão et al. 2013). The specific surface area was calculated using the BET equation, and the total pore volume was estimated from the amount of nitrogen adsorbed at a relative pressure of $P/P_0 = 0.98$. The surface area, average pore diameter, and average pore volume of SnO_2 nanoparticles were determined to be 31.3 m^2 g^{-1}, 2.87 nm, and 0.079 cm^3 kg^{-1}, respectively. These values for AD-GNS were 29.7 m^2 g^{-1}, 2.02 nm, and 0.070 cm^3 kg^{-1}, respectively. Note that pore volume and S_{BET} of AD-GNS decreased in comparison with SnO_2 nanoparticles. This may be a result of the increase in particle size, penetration, and agglomeration, all of which occurs in surface

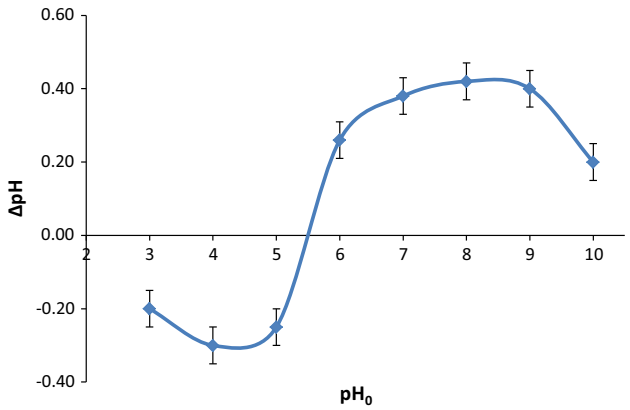

Fig. 3 pH_{PZC} for BNS AD-GNS

modification and grafting stages. The surface area of AD-GNS is small in comparison with adsorbents such as activated carbons but the presence of wider pores favors higher adsorption capacities, especially for large xylene molecules (Ip et al. 2009).

Zeta potential is a physical parameter used to determine the surface electrical potential of a solid particle and the stability of liquid dispersions (Zhang et al. 2013). The point of zero charge (pH_{PZC}) indicates the pH at which the adsorbent material has zero net surface charge (Gusmão et al. 2013). The surface of the material is neutral when $pH = pH_{zpc}$. When $pH < pH_{PZC}$, the adsorbent surface is positively charged, and when $pH > pH_{PZC}$, the surface is negatively charged (Nouri et al. 2002). Figure 3 indicates that pH_{PZC} for AD-GNS was 5.3.

Sorption

One important parameter influencing adsorption is solution pH, which affects the aqueous chemistry and surface binding sites of the adsorbent (Hameed and El-Khaiary 2008). The degree of xylene sorption by pH value was determined using the batch equilibration technique at pH values ranging from 3 to 8 using 0.01 M acetic acid or phosphate buffer. Figure 4a shows the effect of solution pH on the sorption of xylene. It is evident that adsorbate uptake depended on solution pH and that maximum adsorption was achieved at a pH of 5, when $pH_{PZH} = 5.3$. As seen, the optimized solution pH was approximately equal to pH_{PZH}. When $pH = pH_{PZH}$, the surface charge of AD-GNS falls to zero; because xylene has a neutral surface in water, it is easily attracted to the surface of the AD-GNS.

The effect of contact time on the adsorption of xylene was evaluated at initial concentrations of 3, 5, and 8 μg l^{-1} xylene and an optimized pH of 5. The AD-GNS was held constant. Figure 4b shows the adsorption data for xylene uptake by AD-GNS. As seen, xylene uptake was rapid at the beginning in response to the large surface area (29.7 m^2 g^{-1}) with functionalized and available active sites, but then slowed. The adsorption rate became constant as the active sites were covered with xylene and equilibrium was attained. Figure 4b shows that, at lower initial concentrations, adsorption was faster and that 5 min was usually sufficient for 100 % sorption. This reflects good accessibility to active sites on the sorbent. Studies have shown that this was about 15 min for the air stripping and granular active charcoal methods, which are used widely for xylene removal (Shim et al. 2002).

The influence of temperature on xylene sorption by AD-GNS was evaluated, and the results are shown in Fig. 4c. Adsorption capacity increased as temperature increased, indicating higher temperatures enhance adsorption, which may be an endothermic process (Kul and Koyuncu 2010; Alkaram et al. 2009; Panahi et al. 2009). Previous studies have indicated that this effect appears to be caused by the increase in mobility of the xylene with an increase in temperature (Dogan et al. 2000). Increasing the temperature also provides sufficient energy for interactions at active sites on the surface.

Adsorption isotherm

The experimental data for adsorption of xylene onto grafted nano-SnO_2 obeyed the Langmuir, Freundlich, Temkin, and Redlich–Peterson adsorption isotherms. The linearized Langmuir isotherm can be applied for maximum monolayer adsorption capacity of an adsorbent and is expressed as (Langmuir 1918):

$$c_e/q_e = (1/q_{max}K_L) + (C_e/q_{max}) \quad (2)$$

where q_{max} is the maximum adsorption capacity of AD-GNS for complete monolayer coverage on the surface (mg g^{-1}) and K_L is the Langmuir constant (L mg^{-1}).

The value of the Langmuir parameters, calculated in Eq. (2) and evaluated using the intercepts and the slopes of linear plots of C_e/q_e versus C_e, is shown in Fig. 5a and listed in Table 1. The essential characteristics of the Langmuir equation can be expressed in terms of dimensionless constant separation factor, R_L, calculated as (Mellah and Chegrouche 1997):

$$R_L = 1/(1 + K_L C_0). \quad (3)$$

As shown in Table 1, R_L (0.03) is in the range of 0–1, confirming highly favorable adsorption. The value of q_{max}

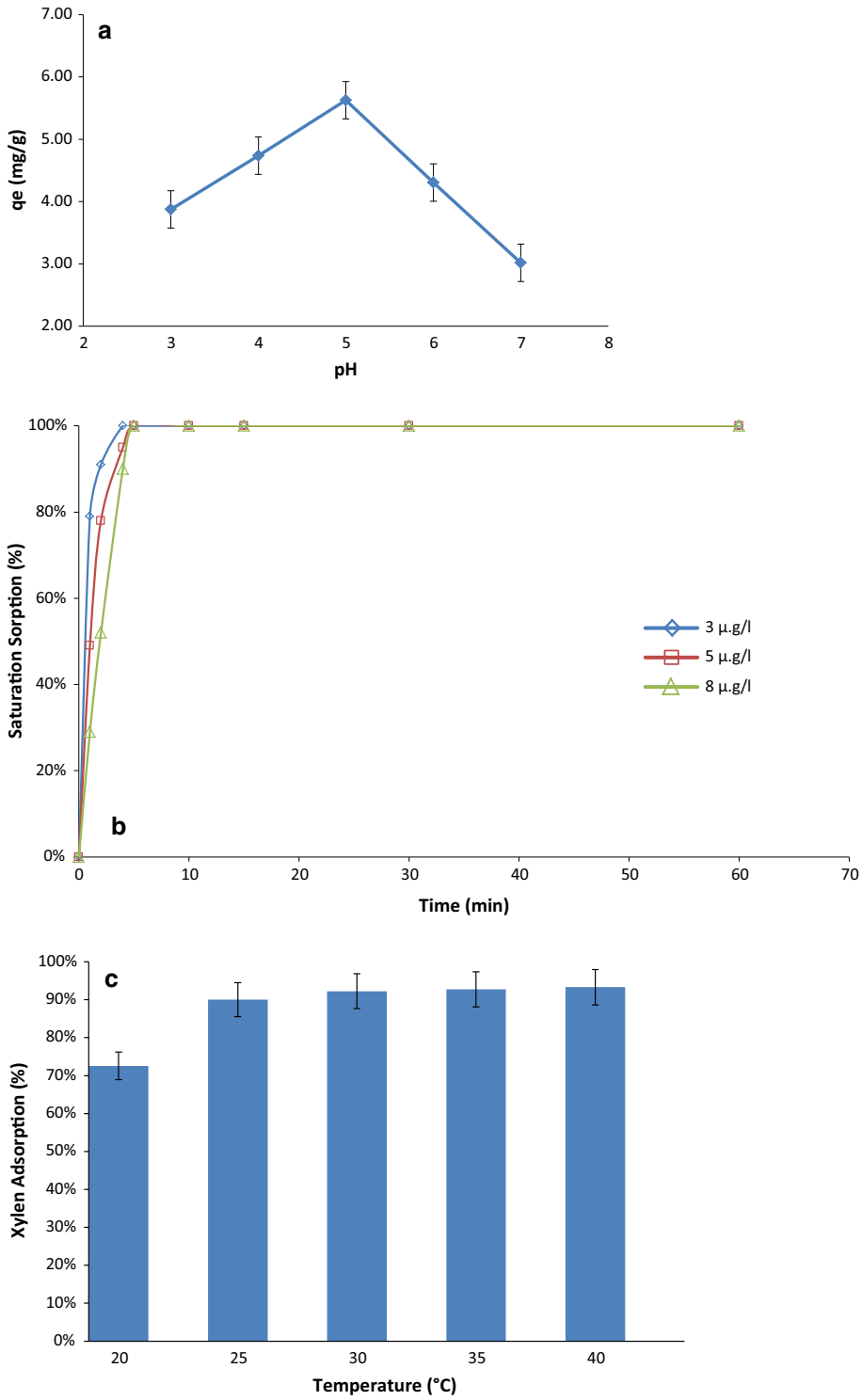

Fig. 4 Effect of: **a** pH; **b** contact time and initial concentration; and **c** temperature on sorption of xylene onto AD-GNS

(8.56) indicates the very high capacity of the synthesized sorbent. According to the different studies, the absorption of xylene from aqueous solutions using different adsorbents is shown in Table 2. The results show that the adsorption capacity of xylene onto activated carbon and modified clay is lower than for AD-GNS, although they

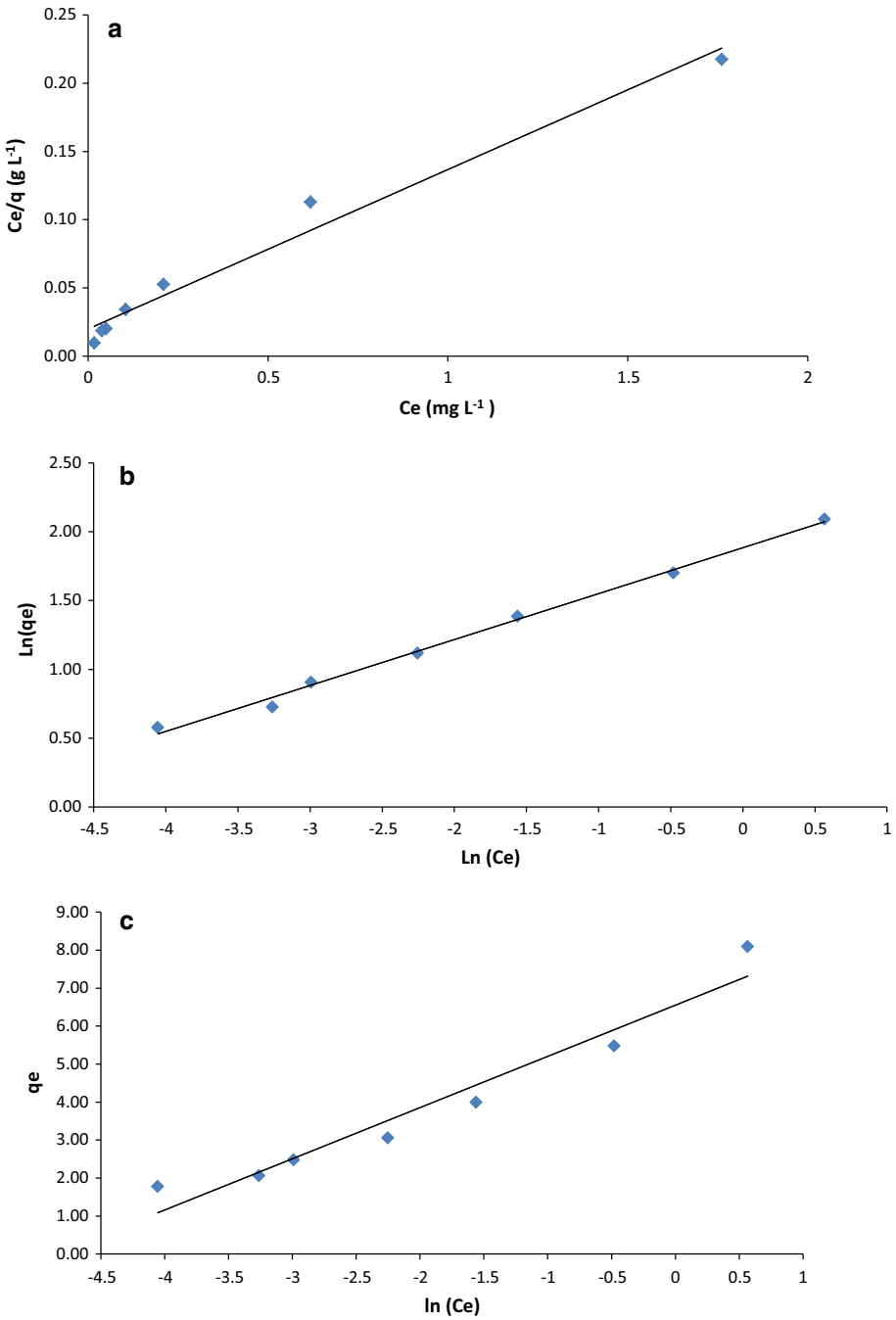

Fig. 5 Adsorption of xylene onto AD-GNS: **a** Langmuir isotherms; **b** Freundlich isotherms; and **c** Temkin isotherms

have higher surface areas. This may be due to the presence of wider pores in AD-GNS, which favors higher adsorption capacities for large xylene molecules.

The Freundlich isotherm is derived empirically and is widely employed to describe multilayer adsorption on a heterogeneous system (Koyuncu et al. 2011; Foo and Hameed 2010). The linearized Freundlich isotherm is expressed as (Madrakian et al. 2012):

$$\ln q_e = \ln K_F = 1/n \ln C_e \quad (4)$$

where K_f(mg g^{-1}) and n are isotherm constants and indicate the capacity and intensity of the adsorption,

Table 1 Isotherm parameters obtained using linear method

Temperature (°C)	q_{max} (mg g^{-1})	K_L	R_L	R^2
Langmuir isotherm model				
25	8.56	5.90	0.03	0.98
Temperature (°C)	K_F (mg g^{-1})	n		R^2
Freundlich isotherm model				
25	6.58	2.99		0.99
Temperature (°C)	A(L g^{-1})	B(J mol^{-1})	B(J mol^{-1})	R^2
Temkin isotherm model				
25	129.62	1.34	1.83	0.94
Temperature (°C)	A(dm^3 m g^{-1})	B(dm^3 m g^{-1})^g	G	R^2
Redlich–Peterson isotherm model				
25	5.0	1.32	1.07	0.99

Table 2 Xylene adsorption from aqueous solutions by different adsorbents

Adsorbent	Capacity (mg g^{-1})	Reference
Adam clay	2.44	Sharmasarkar et al. (2000)
Activated carbon	6.50	Daifullah and Girgis (2003)
TTAB clay	6.98	Nourmoradi et al. (2012)
HDTM clay	7.21	Sharmasarkar et al. (2000)
Grafted SnO_2 nano-sorbent with hydrophobic groups	8.56	This study

respectively, and $1/n$ is the heterogeneity factor and is a function of the strength of adsorption (Njoku et al. 2014). It ranges from 0 to 1 as a measure of adsorption intensity or surface heterogeneity and becomes more heterogeneous as it nears zero (Haghseresht and Lu 1998). A value for n between 1 and 10 indicates that the adsorption bond between adsorbent and adsorbate is strong and also indicates a favorable sorption process (Dada et al. 2012). The n value of (2.99) in this study confirmed that xylene was suitably absorbed by the AD-GNS.

The constants in the Freundlich isotherm, K_f and $1/n$, can be determined by plotting $\ln(q_e)$ versus $\ln(C_e)$ and are shown and listed in Fig. 5b and Table 1, respectively.

The Temkin isotherm contains a factor that explicitly accounts for the adsorbent–adsorbate interaction by suggesting that the fall in the heat of sorption is linear (Foo and Hameed 2010). The equation has generally been applied in the following form:

$$q_e = \mathrm{RT}/b \ln(AC_e) \quad (5)$$

Its linearized form is:

$$q_e = B \ln A + B \ln C \quad (6)$$

where $B = \mathrm{RT}/b$ and b is the Temkin constant for heat of sorption (J mol^{-1}); A is the Temkin constant (L g^{-1}); R is the gas constant (8.314 J mol^{-1} K^{-1}); and T is the absolute temperature (K). Plotting q_e versus $\ln(C_e)$ provides A and B (Fig. 5c). The results are shown in Table 1.

The Redlich–Peterson isotherm is a hybrid isotherm that combines elements of the Langmuir and Freundlich isotherms; its linearized form is (Foo and Hameed 2010):

$$\ln(A(C_e/q_e) - 1) = g \ln C_e + \ln B \quad (7)$$

where A, B, and g are three isotherm constants and can be determined by using trial and error by computer. If g is close to unity, the isotherm approaches Langmuir, and, if it is close to zero, the Freundlich isotherm is dominant. As shown in Table 1, $g = 1.07$; thus, the Langmuir isotherm model better fits the experimental results (Ahmad Panahi et al. 2013). Many studies have indicated that xylene sorption from aqueous solutions by different sorbents is described better by the Langmuir isotherm model (Cheng et al. 2004; Su et al. 2010).

Adsorption kinetics

A suitable kinetic model was needed to analyze the data and investigate the mechanism of adsorption and efficiency of xylene removal. The pseudo-first-order, pseudo-second-order, and intra-particle diffusion models were applied to describe the xylene adsorption mechanism. The pseudo-first-order kinetic model (Bulut et al. 2007) is:

$$\ln(q_e - q_t) = \ln q_e - k_1 t \quad (8)$$

where q_e (mg g^{-1}) is the amount of xylene adsorbed onto AD-GNS at equilibrium and q_t (mg g^{-1}) is the amount adsorbed at any time (t); k_1 (min^{-1}) is the rate constant of the pseudo-first-order kinetic model. The values of k_1 and q_e were calculated from the slope and intercept of $\ln(q_e - q_1)$ and t, respectively, and are listed in Table 3.

The pseudo-second-order model was fit to the adsorption data as:

$$t/q_t = 1/k_2 q_e^2 + t/q_e \quad (9)$$

Table 3 Kinetic parameters for the adsorption of xylene onto AD-GNS

C_0	Q_e exp	Pseudo-first order			Pseudo-second order			
		K_1	Q_e	R^2	K_2	Q_e	R^2	h
3	5.62	0.01	7.03 ± 0.42	0.19	1.09 ± 0.08	5.65 ± 0.32	0.99	34.9 ± 0.13
5	5.64	0.02	6.55 ± 0.38	0.22	0.45 ± 0.01	5.68 ± 0.33	0.99	14.5 ± 0.11
8	5.62	0.03	5.87 ± 0.30	0.25	0.16 ± 0.01	5.77 ± 0.36	0.99	5.49 ± 0.12

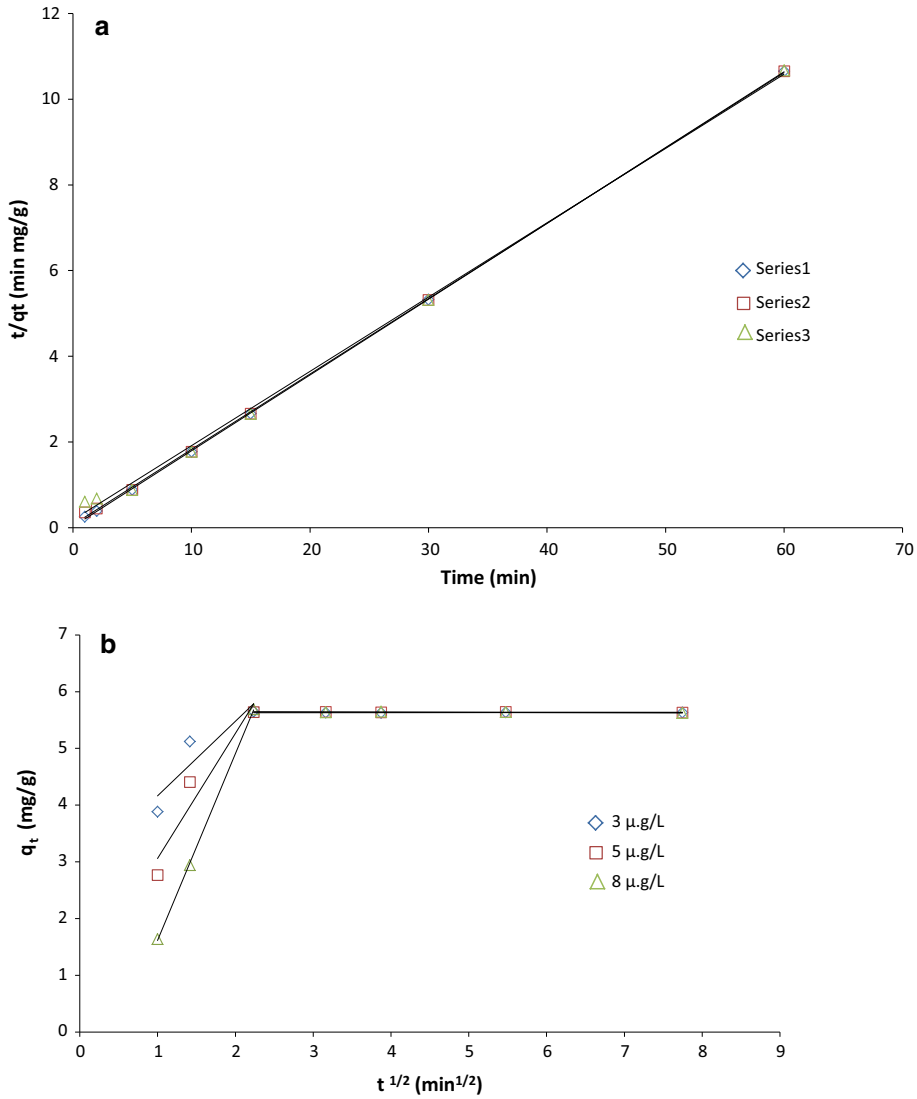

Fig. 6 Modeling of adsorption of xylene onto AD-GNS **a** pseudo-second-order model; **b** intra-particle diffusion model

where k_2 (g mg^{-} min) is the equilibrium rate constant of the pseudo-second order. Figure 6a shows the slopes and intercepts of plots for t/q and t applied to calculate the values of k_2 and q_e (Ho and McKay 1999).

The correlation factors listed in Table 3 indicate that the pseudo-second-order model fits the experimental data better than the pseudo-fist-order model. There was agreement between the q_e calculated by the pseudo-second-order

Table 4 Results of xylene removal from water sample

Sample	Xylene removal (%)	SD	Relative SD (%)[a]
Water sample from Caspian Sea	91	0.6	0.6
Water sample from Persian Gulf	94	2.5	2.7
Water sample from Well water	90	1.5	1.7

[a] For three determinations

kinetic model and the experimental q_e, indicating that the pseudo-second-order model better represented the adsorption kinetics. Researchers have reported that the sorption of xylene with raw and thermally modified diatomite and TTAB-MT is well described by the pseudo-second-order model (Nourmoradi 2012).

Initial sorption rate h (mg g^{-1} min) can be calculated at the initial stage of adsorption ($t \rightarrow 0$) as:

$$h = k_2 q_e^2. \quad (10)$$

Adsorption mechanism

The kinetic experimental data were fit to the intra-particle diffusion model to determine the adsorption mechanism and rate controlling steps, which affect the kinetics of adsorption (Njoku et al. 2014). The kinetic results were analyzed by intra-particle diffusion to examine the diffusion mechanism. Webber and Morris (Su et al. 2011) determined rate constant C and intra-particle diffusion k_{dif} (mg g^{-1} $min^{1/2}$) as:

$$q_t = k_{dif}\sqrt{t} + C. \quad (11)$$

The linear relationship between adsorbate uptake q_t and $t^{1/2}$ indicates that the intra-particle diffusion is rate limited. k_{dif} is calculated from the slope of the linear plot of q_t versus $t^{1/2}$. Figure 6b shows that the first linear stage is sharper and can be attributed to the mass transfer of xylene through the solution to the external surface of the AD-GNS and the second stage can be attributed to the diffusion of xylene molecules inside the AD-GNS.

The value of k_{dif} of the first stage was higher than for the second stage, indicating that the adsorption rate of xylene was higher at the beginning because of the large surface area and large number of mesoporous active sites available for adsorption. In the final equilibrium stage, xylene gradually formed a thick layer in response to inner attraction impedes further adsorption.

Application of method

AD-GNS was used for xylene adsorption in different water samples. The pH of the water samples was adjusted to the optimum pH of 5. Xylene adsorption was recorded by UV/Vis spectrophotometer. When xylene was no longer detected in the water, 100 ml of the water sample was spiked with xylene to prepare a 5 ppm solution before testing.

The water samples were taken from the Caspian Sea (Anzali coast, Gilan, Iran), from the Persian Gulf (Mahshahr coast, Booshehr, Iran), and from well water (Africa St., Tehran, Iran). The results are shown in Table 4 and demonstrate the applicability of proposed procedure for xylene adsorption.

Conclusion

A new sorbent synthesized by free radical graft copolymerization of ABE and DMAA onto modified nano-SnO_2 with 3-mercaptopropyl trimethoxysilane was used to adsorb xylene from aqueous media. The synthesis of the sorbent is simple and economical, but the modification stage is time consuming. Although the sorbent could not be regenerated, it showed high thermal and chemical stability and high capacity for polymer grafting.

Research indicates that the sorption of xylene was much better fitted to the Langmuir isotherm model, and the maximum adsorption capacity was about 8.56 mg g^{-1}. Two adsorption kinetic models were evaluated, and the pseudo-second-order model fits the experimental data better than did the pseudo-first-order model. The adsorption mechanism was studied using an intra-particle model which indicated that xylene adsorption onto AD-GNS involves more than one kinetic stage. The sorbent was successfully applied to xylene removal from environmental samples and was shown to adsorb more than 90 % of the xylene in the samples.

Acknowledgments The authors would like to express their gratitude to the Science and Research branch of Islamic Azad University for providing the facilities to carry out this research.

References

Ahmad Panahi H et al (2010) Grafting of poly [1-(N, N-bis-carboxymethyl) amino-3-allylglycerol-co-dimethylacrylamide] copolymer onto siliceous support for preconcentration and determination of lead (II) in human plasma and environmental samples. J Chromatogr A 1217(32):5165–5172

Ahmad Panahi H et al (2013) Synthesis and characterization of poly [1-(N, N-bis-carboxymethyl) amino-3-allylglycerol-co-dimethylacrylamide] grafted to magnetic nano-particles for extraction and determination of letrozole in biological and pharmaceutical samples. Talanta 117:511–517

Aivalioti M et al (2010) BTEX and MTBE adsorption onto raw and thermally modified diatomite. J Hazard Mater 178(1):136–143

Aivalioti M et al (2012a) Adsorption of BTEX, MTBE and TAME on natural and modified diatomite. J Hazard Mater 207:117–127

Aivalioti M et al (2012b) Removal of BTEX, MTBE and TAME from aqueous solutions by adsorption onto raw and thermally treated lignite. J Hazard Mater 207:136–146

Alkaram UF et al (2009) The removal of phenol from aqueous solutions by adsorption using surfactant-modified bentonite and kaolinite. J Hazard Mater 169(1):324–332

Bulut Y et al (2007) Equilibrium and kinetics studies for adsorption of direct blue 71 from aqueous solution by wheat shells. J Hazard Mater 144(1):300–306

Chaimberg M, Cohen Y (1990) Note on the silylation of inorganic oxide supports. J Colloid Interface Sci 134(2):576–579

Cheng B et al (2004) Large-scale, solution-phase growth of single-crystalline SnO2 nanorods. J Am Chem Soc 126(19):5972–5973

Chiefari J et al (2003) Thiocarbonylthio compounds (SC (Z) SR) in free radical polymerization with reversible addition-fragmentation chain transfer (RAFT polymerization). Effect of the activating group Z. Macromolecules 36(7):2273–2283

Dada A et al (2012) Langmuir, Freundlich, Temkin and Dubinin-Radushkevich Isotherms Studies of Equilibrium Sorption of Zn2+ Unto Phosphoric Acid Modified Rice Husk. IOSR J Appl Chem 3(1):38–45

Daifullah A, Girgis B (2003) Impact of surface characteristics of activated carbon on adsorption of BTEX. Colloids Surf A 214(1):181–193

Doğan M et al (2000) Adsorption of methylene blue from aqueous solution onto perlite. Water Air Soil Pollut 120(3–4):229–248

El-Etre A, Reda S (2010) Characterization of nanocrystalline SnO₂thin film fabricated by electrodeposition method for dye-sensitized solar cell application. Appl Surf Sci 256(22):6601–6606

Foo K, Hameed B (2010) Insights into the modeling of adsorption isotherm systems. Chem Eng J 156(1):2–10

Fujihara S et al (2004) Hydrothermal routes to prepare nanocrystalline mesoporous SnO2 having high thermal stability. Langmuir 20(15):6476–6481

Gaber A et al (2013) Thermally induced structural changes and optical properties of tin dioxide nanoparticles synthesized by a conventional precipitation method. Mater Sci Semicond Process 16(6):1784–1790

Gusmão KAG et al (2013) Adsorption studies of methylene blue and gentian violet on sugarcane bagasse modified with EDTA dianhydride (EDTAD) in aqueous solutions: kinetic and equilibrium aspects. J Environ Manag 118:135–143

Haghseresht F, Lu G (1998) Adsorption characteristics of phenolic compounds onto coal-reject-derived adsorbents. Energy Fuels 12(6):1100–1107

Hameed B, El-Khaiary M (2008) Malachite green adsorption by rattan sawdust: isotherm, kinetic and mechanism modeling. J Hazard Mater 159(2):574–579

Ho Y-S, McKay G (1999) Pseudo-second order model for sorption processes. Process Biochem 34(5):451–465

Ip A et al (2009) Reactive Black dye adsorption/desorption onto different adsorbents: effect of salt, surface chemistry, pore size and surface area. J Colloid Interface Sci 337(1):32–38

Kee WK et al (2014) Erratum to: self-immobilised bacterial consortium culture as ready-to-use seed for crude oil bioremediation under various saline conditions and seawater. Int J Environ Sci Technol 11(7):2119

Koyuncu H et al (2011) Adsorption of o-, m-and p-nitrophenols onto organically modified bentonites. J Hazard Mater 185(2):1332–1339

Kul AR, Koyuncu H (2010) Adsorption of Pb(II) ions from aqueous solution by native and activated bentonite: kinetic, equilibrium and thermodynamic study. J Hazard Mater 179(1):332–339

Langmuir I (1918) The adsorption of gases on plane surfaces of glass, mica and platinum. J Am Chem Soc 40(9):1361–1403

Liang Y et al (2007) Synthesis and characterisation of SnO₂nano-single crystals as anode materials for lithium-ion batteries. Mater Lett 61(22):4370–4373

Lin SH, Huang CY (1999) Adsorption of BTEX from aqueous solution by macroreticular resins. J Hazard Mater 70(1):21–37

Madrakian T et al (2012) Adsorption and kinetic studies of seven different organic dyes onto magnetite nanoparticles loaded tea waste and removal of them from wastewater samples. Spectrochim Acta Part A Mol Biomol Spectrosc 99:102–109

Mellah A, Chegrouche S (1997) The removal of zinc from aqueous solutions by natural bentonite. Water Res 31(3):621–629

Njoku V et al (2014) Utilization of sky fruit husk agricultural waste to produce high quality activated carbon for the herbicide bentazon adsorption. Chem Eng J 251:183–191

Nouri S et al (2002) Adsorption of aromatic compounds by activated carbon: effects of functional groups and molecular size. Adsorpt Sci Technol 20(1):1–15

Nourmoradi H et al (2012) Multi-component adsorption of benzene, toluene, ethylbenzene, and xylene from aqueous solutions by montmorillonite modified with tetradecyl trimethyl ammonium bromide. Journal of Chemistry 2013:1–10

Organization WH (2004) Guidelines for drinking-water quality: recommendations, World Health Organization

Panahi HA et al (2009) Amberlite XAD-4 functionalized with m-phenylendiamine: synthesis, characterization and applications as extractant for preconcentration and determination of rhodium (III) in water samples by Inductive Couple Plasma Atomic Emission Spectroscopy (ICP-AES). Microchem J 93(1):49–54

Panahi HA et al (2013) Synthesis and characterization of new molecular imprinting poly [1-(N, N-bis-carboxymethyl) amino-3-allylglycerol-co-dimethylacrylamide] for selective sorption and determination of cefuroxime sodium in biological and pharmaceutical samples. React Funct Polym 73(1):132–140

Paraguay-Delgado F et al (2005) Structural analysis and growing mechanisms for long SnO2 nanorods synthesized by spray pyrolysis. Nanotechnology 16(6):688

Shahriari T et al (2014) Effective parameters for the adsorption of chromium (III) onto iron oxide magnetic nanoparticle. Int J Environ Sci Technol 11(2):349–356

Sharmasarkar S et al (2000) BTEX sorption by montmorillonite organo-clays: TMPA, ADAM, HDTMA. Water Air Soil Pollut 119(1–4):257–273

Shim H et al (2002) A continuous fibrous-bed bioreactor for BTEX biodegradation by a co-culture of Pseudomonas putida and Pseudomonas fluorescens. Adv Environ Res 7(1):203–216

Silva-Castro G et al (2012) Treatment of diesel-polluted clay soil employing combined biostimulation in microcosms. Int J Environ Sci Technol 9(3):535–542

Su F et al (2010) Adsorption of benzene, toluene, ethylbenzene and p-xylene by NaOCl-oxidized carbon nanotubes. Colloids Surf A 353(1):83–91

Su J et al (2011) Adsorption of phenol from aqueous solutions by organomontmorillonite. Desalination 269(1):163–169

Vieira AP et al (2009) Kinetics and thermodynamics of textile dye adsorption from aqueous solutions using babassu coconut mesocarp. J Hazard Mater 166(2):1272–1278

Ying Z et al (2004) SnO2 nanowhiskers and their ethanol sensing characteristics. Nanotechnology 15(11):1682

Zhang Y et al (2013) Sorption and removal of tetrabromobisphenol A from solution by graphene oxide. Chem Eng J 222:94–100